Archaeol Anthropol Sci
DOI 10.1007/s12520-011-0080-1

ORIGINAL PAPER

Ceramic findings from the archaeological site at Aiano-Torraccia di Chiusi (Siena, Italy): a multi-analytical approach

E. Cantisani · M. Cavalieri · C. Lofrumento · E. Pecchioni · M. Ricci

Received: 20 December 2010 / Accepted: 26 September 2011

Abstract In 2005, the remains of a Roman *villa*, dating from the early fourth to the sixth centuries AD, were discovered at the archaeological site of Aiano-Torraccia di Chiusi (Siena, Italy). After being abandoned in the sixth century AD, the complex was occupied by a group of Ostrogothic or Lombardic artisans in the period between the sixth and the seventh centuries AD. Many ceramic remains (coarse pottery and red slip ceramics) from the first to the seventh centuries AD have been discovered on this archaeological site. These findings have been analysed using different analytical techniques (optical microscopy (OM), X-ray diffraction (XRD), X-ray fluorescence (XRF), scanning electron microscope-energy dispersive spectroscopy (SEM-EDS), attenuated total reflection Fourier transform infrared (ATR-FTIR), and micro-Raman in order to characterize the ceramic body, the coating, the temper, and to investigate the compositional relationship between the different kinds of ceramics. The use of different techniques on the same samples yielded information at different scales. OM and SEM-EDS yielded interesting information on the coarse pottery: the analyses performed on some minerals and rock fragments suggest that stone *tesserae* from the Roman *villa* (in the form of numerous marble fragments) were used in the production of this pottery. Bulk analyses (XRD and XRF) and subsequent micro-analyses (SEM-EDS, ATR-FTIR, and micro-Raman) of the red slip pottery revealed clear chemical, mineralogical and textural differences: some ceramics (the TCC sample group) typically have a Fe-enriched coating while others (the INGR sample group) present a clear difference in grain size but no chemical or mineralogical differences between the ceramic body and the coating.

Keywords Aiano-Torraccia di Chiusi (Siena) · Red slip ceramics · Coarse pottery · SEM-EDS · ATR-FTIR · Raman · XRD · XRF · OM

E. Cantisani (✉)
CNR-ICVBC Institute for Conservation and Enhancement of Cultural Heritage,
Via Madonna del Piano 10,
Sesto Fiorentino, Florence, Italy
e-mail: e.cantisani@icvbc.cnr.it

M. Cavalieri
Department of Archaeology and History Art,
Institute for Civilizations, Arts and Literature Université catholique de Louvain (UCL) Place B. Pascal,
1 Collège Erasme, P.O. Box L3.03.13, 1348 Louvain-la-Neuve, Belgium
e-mail: marco.cavalieri@uclouvain.be

C. Lofrumento
Department of Chemistry, University of Florence,
Via Della Lastruccia 3,
50019 Sesto Fiorentino, Florence, Italy

E. Pecchioni
Department of Earth Sciences, University of Florence,
Via G. La Pira 4,
50121 Florence, Italy

M. Ricci
Department of Construction and Restoration,
University of Florence,
Via Micheli 8,
50121 Florence, Italy

Introduction

A Belgian-Italian mission of the *Université catholique de Louvain* has been excavating an archaeological site located in a marginal area of the *Ager Volaterranus* since 2005. During the last five campaigns, an articulated settlement

Published online: 14 October 2011

has been brought to light in this area which is well known for significant discoveries that date to Roman times. This settlement consists of a *villa longinqua* with monumental architecture and decorative apparatus that was probably built between the end of the third and the beginning of the fourth century AD. A hexalobate hall, surrounded by a monumental pentalobate *ambulatio* that was accessed through a rectangular vestibule, belongs to this first phase.

The hall, *ambulatio* and vestibule played an important role in connecting different parts of the building: this characteristic, highlighted by the coaxial openings at the ends of the hall, is found in other contemporary buildings, for example the *Cazzanello villa* near Tarquinia.

In a later period—dated stratigraphically to the last quarter of the fourth century AD—the *villa* was heavily restored following a natural traumatic event. In particular, the hexalobate hall was radically transformed, both architectonically and functionally: the floor was lowered considerably and three exedras were destroyed and substituted by three rectangular rooms. This new arrangement resulted in an unusual shape: a trilobate hall with a triangular base, very different from the classic *trìkonchos*. The new floor of the hall was paved with *opus signinum*: there were geometric decorations in the centre of the hall and in the apse in front of the vestibule; the other two apses had a central ornamental *emblema* (the best preserved represents a flowered goblet placed in a *guilloche* framed by a denticulate arch) (Cavalieri 2009a).

Even though the hall lost its function as a passageway during this phase, becoming a room reserved for *otium*, the external *ambulatio* retained its function. The structure showed the first traces of disuse and collapse during the fifth century AD: presumably some parts (like the trilobate hall) were abandoned and progressively hidden by the collapse of the parietal panels and the roof structure. Other parts were subjected to the first depredations for recovering marbles for use elsewhere.

Only in a later period when the *villa*, was already in ruins, it was used as a quarry for various materials (iron, copper, gold, and vitreous pastes) destined for the production of small objects such as pins, bracelets and necklace beads. During this phase, the rectangular rooms, built outside the trilobate hall, were used as small workshops for the manufacture of pottery (room H) and gold (room L) and bronze (room I) objects while the rooms on the southern side accommodated workshops for manufacturing glazes (vestibule, room A) and objects made of iron (room B) (Cavalieri and Giumlia-Mair 2009) (Fig. 1).

During the second half of the seventh century AD, the excavated part of the structure was definitively abandoned, although there is evidence that this area was frequented during the Late Middle Ages. The presence of people passing not far from the *villa* was probably due to the deviation of the Francigena Road (or Via Romea), as testified by Sigeric, Archbishop of Canterbury, who travelled through this area at the end of the tenth century (Cavalieri 2009b).

The ceramic findings at Aiano-Torraccia di Chiusi include coarse pottery, depurated ceramic with a red/brown slip, uncoated depurate, semi-depurate, lamps, amphorae and *dolia.* There are also residual elements, mostly external to the context of the excavation: for example fragments of a *Kelebe* from Volterra dated to the III BC, black gloss pottery from the fourth–fifth BC, frustules of protohistoric paste and a very few tiny fragments of Italic *Sigillata* located in the stratigraphic sequences. These finds have made a detailed investigation necessary: firstly to study the phases of frequentation of the area prior to the construction of the *villa* and secondly, and more importantly, to study the role played by the *villa* from the second half of the fifth to the late seventh centuries when it was abandoned. In particular this work focuses on the study of a significant number of ceramic findings (dated from the fifth to seventh AD), to facilitate an understanding of the role the *villa* played as a site of production activities and how its constituent materials (i.e. mosaics and decorative elements) were reutilized. The principal objectives of this paper are to characterize the ceramic body and coating of the red slip ceramics, the matrix and temper of the coarse pottery in order to investigate the compositional relationship between these two different kinds of ceramics and to use this information to assess whether both typologies were produced locally. This paper also evaluates the extent to which different techniques can provide information relative to a given sample at different scales.

Materials and analytical methods

A description of the types of the ceramic findings analysed is reported below (Fig. 2a, b; Table 1), followed by a presentation of the analytical methods.

The samples of these findings consist of coarse uncoated pottery (AG) and red slip ceramics. The red slip ceramic samples are subdivided into INGR samples and TCC or "similar to African" samples. This last definition has been used to identify a few ceramic fragments found in the *villa* that have a different morphology from the red slip ceramics. It is difficult to assess whether these fragments can be classified as African red pottery although it is highly probable given their tiny size.

Red slip ceramics

The pottery found in the area is a typical representation of the production known in Tuscany between the fifth and

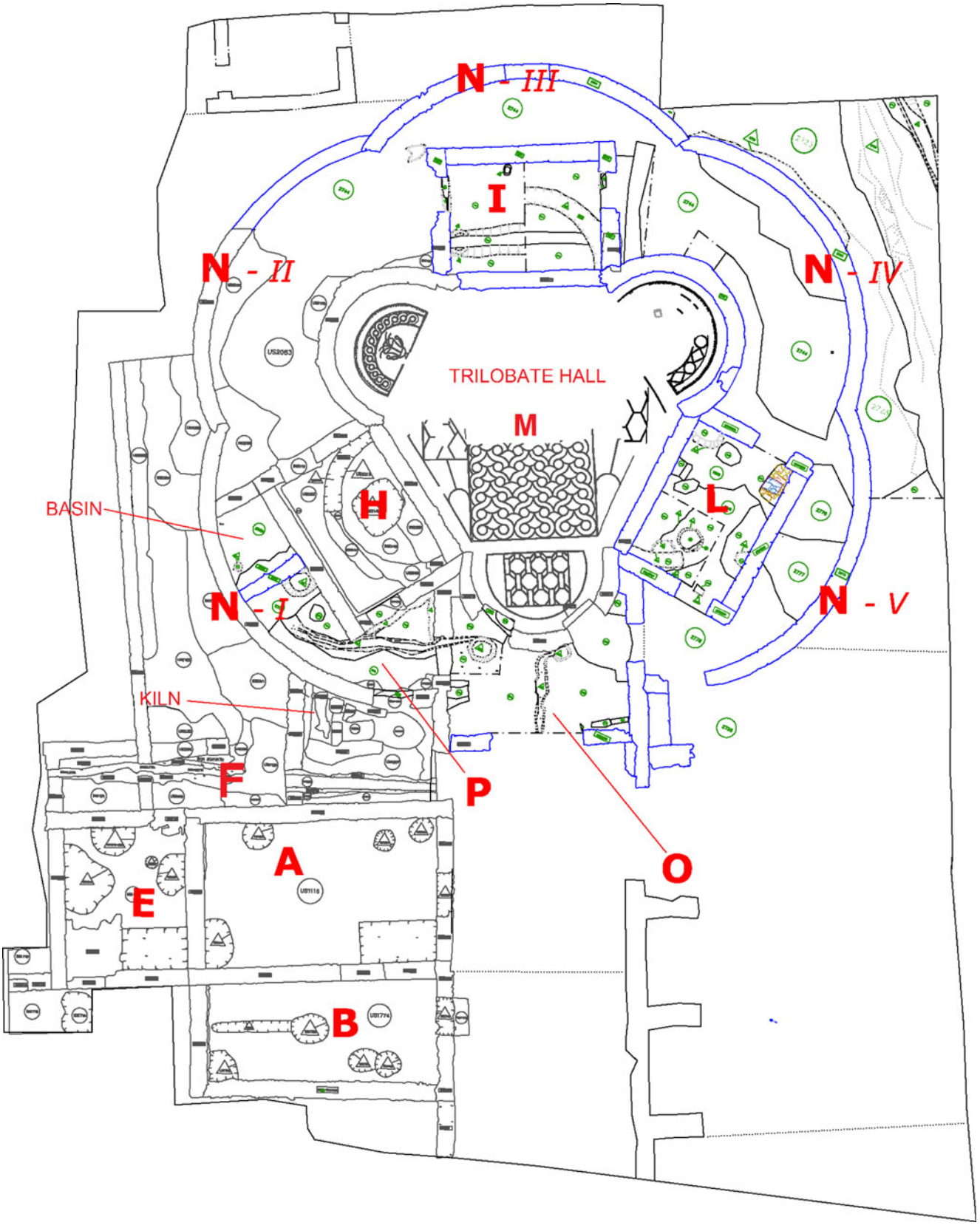

Fig. 1 Map of archaeological site in the summer 2009 with the indication of rooms name

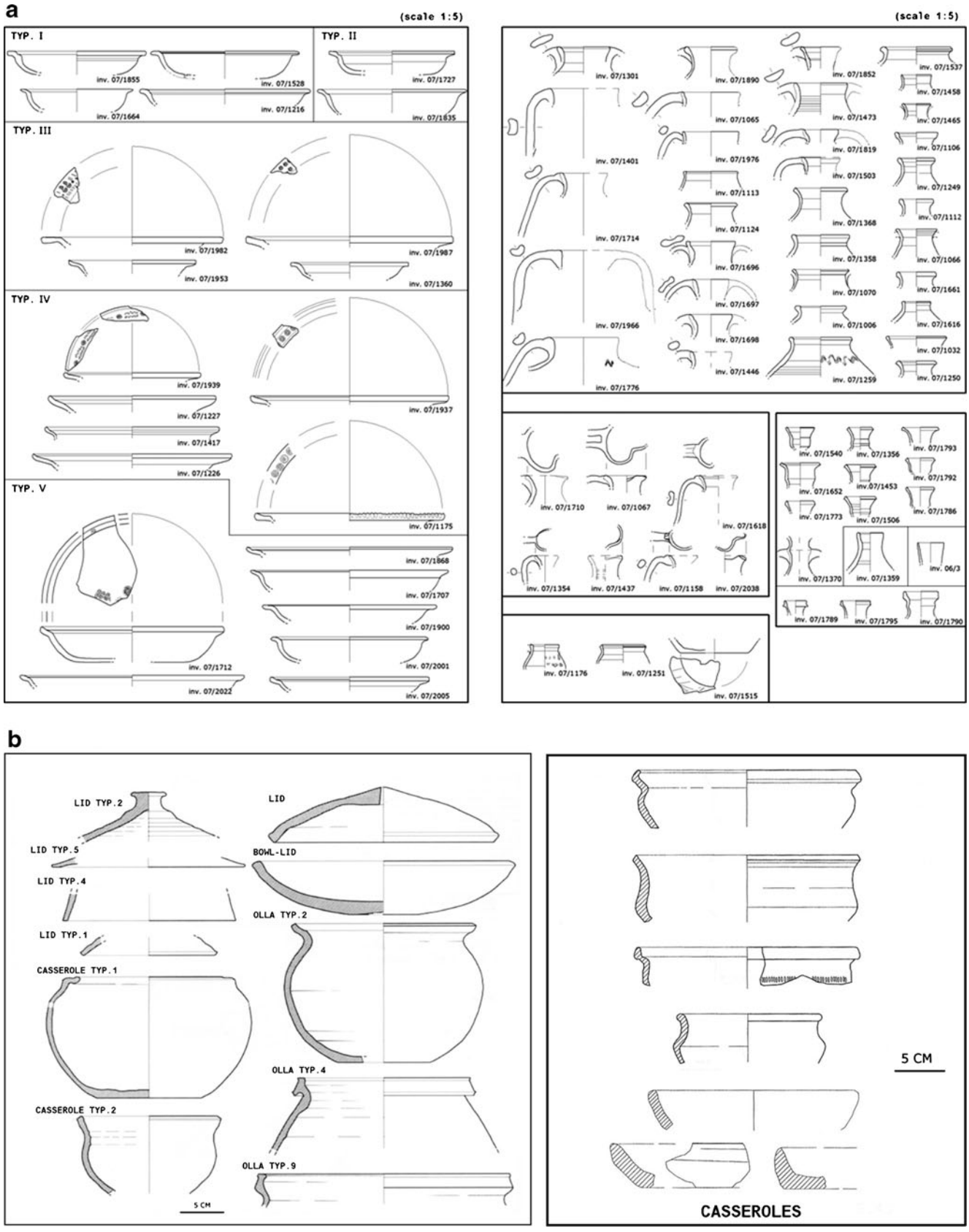

Fig. 2 Shape and typologies of red slip ceramics (INGR samples): plates trays (*left*), closed shapes (*right*) (**a**); coarse pottery (AG samples) (**b**) (drawn by Antonia Fumo and Enrica Boldrini)

Table 1 List of red slip ceramics (INGR and TCC) and coarse pottery (AG) with indication of strathigraphic unit (US), location and shape

Sample	US	Room	Shape
INGR 2	1112	Room E	Closed shape
INGR 4	1085	Room E	Jug
INGR 5	1085	Room E	Closed shape
INGR 9	1101	Room A	Closed shape
INGR 10	1101	Room A	Closed shape
INGR 14	1012	Room A	Closed shape
INGR 24	2090	Kiln Room	Plate tray
INGR 25	2090	Kiln Room	Plate tray
INGR 26	2136	Trilobate hall	Plate tray
INGR 27	2090	Kiln hall	Plate tray
INGR 28	2081	NW sector	Plate tray
TCC 2136	2136	Trilobate hall	Wall of cup
TCC 2157	2157	Trilobate hall	Wall of cup
AG 2	1104	Room E	Cooking pot
AG 4	1103	Room E	Casserole
AG 23	1098	Room A	Cooking pot
AG 28	1089	Room A	Bowl lid
AG C4A	2130	Trilobate hall	Lid
AG C5	2130	Trilobate hall	Lid
AG C6	2074	NW sector	Bowl lid
AG C7	2074	NW sector	Bowl lid
AG C8	1088	Room E	Bowl lid
AG C9	1088	Room E	Bowl lid
AG C10	1098	Room A	Bowl lid
AG C11	2041	Room F	Bowl lid
AG C13	2094	Kiln Room	Bowl lid
AG 32	2001	Room M	Cooking pot
AG 33	2090	Room M	Cooking pot
AG 34	2090	Room M	Cooking pot
AG 35	2090	Room M	Cooking pot
AG 36	2090	Room M	Small handles pots
AG 37	2120	Room M	Cooking pot
AG 38	2130	Room M	Cooking pot
AG 39	2130	Room M	Cooking pot
AG 40	2157	Room M	Bowl

seventh centuries AD. In fact coarse pottery, red slip pottery, depurated and semi-depurated wares are all present (Fumo 2010). Generally, red slip pottery represents a stylistic imitation, often on a regional basis, of Late African Red Slipware, present from as early as the second to the fourth centuries AD until the seventh century AD. After the seventh century AD there was a process of transformation and the typologies produced in Tuscany gradually acquired specific autonomous characteristics that distinguished them from the typologies produced in other parts of Italy during the same period.

Closed shapes Many shapes have been discovered: jugs (some of them trilobate), mugs, small amphorae, bottles, flasks, and glasses. Despite this, it has been possible to determinate the chronological period in which these shapes were produced, from the fifth to the seventh centuries AD, and their distribution in the excavated area.

Plates trays Together with bowls and cups they are the most common red-coated pottery objects found on the site of the *villa*. The plate trays have ample diameters, quite low sides and are footless; they were generally used as dinner plates. The vases imitate the Hayes 42 and 45 shapes of Late African Red Slipware (Hayes 1972). Their production can be dated to sometime between the fifth and the seventh centuries AD.

Uncoated ceramics (coarse pottery)

All the typologies are represented in the coarse pottery remains: cooking pots (*olle*), bowl lids, casseroles, lids, jugs, and small jugs. The cooking pots are of a medium/small size and often have very fine threading on the back and one or more engraved lines for identifying the start of the neck. The casserole is a peculiar typology for this chronological range. Cooking pots and casseroles have smoothed external sides and detached bases with a blade. They have widespread blackening both externally and internally due to manufacturing and/or contact with fire and coal. The lids are classified in six typologies, based on their thickness and height. They were produced on a fast wheel and sometimes smoothed; they rarely show internal or external blackening and their diameters are compatible with those of the cooking pots and casseroles.

Some fragments of medium and small-sized jugs have also been identified. The fragments are of thin smoothed walls with external and internal blackening, parts of the upper border and parts of mostly small-sized nozzles. The bow lids have a typical crushed-cap shape with a small groove. They are large and of an appropriate thickness, their surfaces are rough and they were made with coarse pastes (Cavalieri and Boldrini 2008). They too, can be dated to between the fifth and seventh centuries AD.

Analytical methods

Diverse analytical techniques were used in order to obtain useful and representative analyses for each type of ceramic finding. The techniques chosen were selected because they could provide the necessary information without requiring redundant and expensive analyses (Maggetti 1982; Maggetti 1994; Fabbri 1998; Tite 1999; Turbanti Memmi 2004;

Cuomo di Caprio 2007; Pecchioni et al. 2007). Most of the data for the red slip ceramics were obtained through bulk chemical and mineralogical petrographical analyses of the ceramic body and coating: X-ray fluorescence (XRF), X-ray diffraction (XRD), optical microscopy (OM). Micro-chemical analyses of each individual ceramic body (attenuated total reflection Fourier transform infrared (ATR-FTIR), and scanning electron microscope-energy dispersive spectroscopy (SEM-EDS)) and of coating (ATR-FTIR, SEM-EDS, and micro-Raman) were performed in order to determine their composition. Much of the data for the coarse pottery (uncoated and with macroscopic added temper) were obtained using OM linked to SEM-EDS analyses. These techniques yielded data on the composition and origin of the added temper.

Not every sample was submitted to all the analyses: i.e. the micro-chemical analyses (SEM-EDS), ATR-FTIR and the micro-Raman analyses were performed only on representative selected samples, while the petrographical and mineralogical analyses were performed on every sample so as to classify and select the samples that would undergo micro-chemical analyses.

X-ray diffraction Powder XRD was adopted to determine the mineralogical composition of the ceramic findings: a Philips PW 1050/37 diffractometer was used with a Philips X'Pert PRO data acquisition system, operating at 40 kV–20 mA, with a Cu anode, a graphite monochromator and with 2°/min goniometry speed in a scanning range between 5–70°.

X-ray fluorescence XRF on pressed-powder pellets was adopted to determine the chemical composition; a Philips PW 1480 wavelength dispersive spectrometer was used; major elements were determined using a Rh anode and estimated using the method adopted by Franzini et al. 1975.

ATR-FTIR Fourier transform infrared spectroscopy was performed on samples of red slip ceramic findings using a Spectrum 100 Perkin Elmer with an attenuated ATR diamond crystal. The detector was fast recovery deuterated L-alanine tryglycine sulphate, and the spectral range was 4,000–380 cm^{-1} with a spectral resolution of 4 cm^{-1}.

Electron microscopy The SEM-EDS analyses were performed with an electron microscope (Zeiss EVO MA 15), coupled to an analytical system (EDS OXFORD INCA 250). The following standards were used for the semi-quantitative analyses: Albite, MgO, Al_2O_3, SiO_2, Wollastonite, MAD-10 Feldspar, Ti, and Fe.

Optical microscopy The petrographic description of samples was carried out using a polarised light microscope (ZEISS Axioskop; OM) on thin sections (30 μm thickness), observed at different magnifications. The microscope was equipped with a camera (resolution, 5 megapixels) and dedicated image analysis software (AxioVision) for evaluating the textural parameters.

Micro-Raman A Renishaw single-grating (1,200 grooves/mm) RM2000 micro-Raman spectrometer was used for Raman measurements. Spectra were recorded using the 785 nm excitation line of a Renishaw air-cooled diode laser. Laser beam focusing was accomplished through a ×50 magnification objective which provided a 1.5-μm laser spot diameter. Neutral density filters were used to attenuate the laser power in order to avoid phase transformations. For each sample, Raman spectra were taken on an average of five randomly selected points on the coated surface of each sample of the ceramic findings. Acquisition times ranged from 10 to 100 s. Spectra were recorded over the range of 200–800 cm^{-1} at step intervals of 1 cm^{-1} and with a 50 μm slit aperture. The instrumental broadening, evaluated as the line width (full width at half-maximum) of an emission line from a He–Ne lamp, was 3 cm^{-1}. Experimental conditions (i.e. magnification and sample illumination) were kept constant for all measurements.

Results and discussion

Red slip ceramics

Table 2 reports the mineralogical composition of the red slip ceramic findings obtained by homogenizing the coating and the ceramic body.

The samples are characterized by the presence of quartz, plagioclases (except TCC 2136 and TCC 2157 which contain K-feldspar but no plagioclases) and hematite (except INGR 28). Pyroxenes are only present in the INGR 2, INGR 4 and INGR 28 samples; calcite is only present in the INGR 24, INGR 25, INGR 26, and INGR 28 samples with traces in the INGR 14 and INGR 27 samples. Phyllosilicates (illite and muscovite) are present in almost all the samples. There are some differences in the mineralogical composition of the INGR and TCC samples but the data are insufficient to obtain precise information about the manufacturing technology used.

Table 3 reports the bulk chemical analyses performed with the XRF method using powder obtained by homogenizing the coating and ceramic body. These data can be considered as a mean composition of these ceramics. The TCC 2136 sample is characterized by higher levels of SiO_2 and lower levels of CaO with respect to the INGR samples. These differences can be attributed to the use of different raw materials for the realization of the TCC and the INGR samples. In the case of CaO (INGR samples), secondary

Table 2 Mineralogical composition (XRD) of red slip ceramic findings

	Quartz	Calcite	Plagioclase	K-feldspar	Hematite	Phyllosilicates	Pyroxene
INGR 2	X	–	X	X	X	Traces	X
INGR 4	X	–	X	–	X	X	X
INGR 5	X	–	X	–	X	X	–
INGR 9	X	–	X	–	X	X	–
INGR 10	X	–	X	X	X	X	–
INGR 14	X	Traces	X	–	X	X	–
INGR 24	X	X	X	–	X	Traces	–
INGR 25	X	X	X	X	X	Traces	–
INGR 26	X	X	X	X	X	X	–
INGR 27	X	Traces	X	X	X	Traces	–
INGR 28	X	X	X	–	–	X	X
TCC 2136	X	–	–	X	X	–	–
TCC 2157	X	–	–	X	X	–	–

phenomena associated with the alteration of buried ceramic findings also need to be investigated.

Mineralogical and chemical analyses, such as XRD and XRF, are very useful for a general characterization of the samples, but, because they are performed on homogenized samples, which contain both coating and body, they do not provide a complete picture of the method of ceramic production and the source of the raw materials. Significant information on production technology was obtained by studying the coating and the body separately: chemical analyses (ATR-FTIR which is sensitive to molecular structure and SEM-EDS for elementary semi-quantitative characterization) were performed on the coating and the ceramic body. The SEM-EDS data are reported in Table 4.

While the chemical composition of the coating of the INGR 4, INGR 14, and INGR 28 samples is quite similar to the composition of the ceramic body, the amount of FeO present in the coating and the ceramic body in the TCC 2136 and TCC 2157 samples ("similar to African") differs considerably; there is more FeO in the coating, suggesting an addition of Fe-rich material so as to obtain a red colour.

The textural information obtained using SEM-EDS reveals that in the INGR 4 and INGR 28 samples (Fig. 3) the grain size of the skeleton of the particles constituting the coating is smaller than in the ceramic body. The coating is less porous and has a smaller amount of CaO due to the absence of secondary $CaCO_3$ which is present in the more porous ceramic body. The ATR-FTIR spectra of the ceramic body and the coating in the INGR 24, INGR 25, and INGR 27 samples were characterized by the presence of calcite, quartz, and aluminosilicate as the main components. All the samples contain calcite in different amounts due to either the probable composition of the raw clay and/or to secondary precipitation phenomena. However, as the most significant absorption peaks of the spectra occur at wave numbers below 1,300 cm^{-1}, only these portions of the spectra are presented and discussed. The characteristic infrared frequencies of minerals identified in the ceramic samples were attributed by correlation data on standard minerals and on the basis of data reported in the literature (Farmer 1974), when it was not possible to have a standard sample of the relevant mineral.

The 1,300–400 cm^{-1} region of the ATR-FTIR spectra of the ceramic bodies of the INGR 24, INGR 25, INGR 27 samples, together with their second derivative profile, is given in Fig. 4a, b. The second derivative of the IR absorption

Table 3 Chemical analyses (XRF) of red slip ceramics (oxide wt.%)

	SiO_2	TiO_2	Al_2O_3	Fe_{tot}	MnO	MgO	CaO	Na_2O	K_2O	P_2O_5	LOI
INGR 5	55.99	0.86	18.00	7.88	0.08	4.12	7.47	0.91	2.64	0.24	1.82
INGR 9	54.56	0.79	16.23	6.80	0.09	3.69	7.82	0.63	2.62	0.27	6.50
INGR 10	60.77	0.81	17.54	7.26	0.07	3.54	4.14	1.01	2.82	0.12	1.91
INGR 14	53.51	1.02	22.37	8.41	0.19	3.36	4.49	0.57	3.33	0.19	2.57
INGR 25	53.90	0.72	15.35	6.74	0.08	3.14	10.69	0.88	2.51	0.36	5.56
INGR 27	55.39	0.81	15.90	7.79	0.06	3.34	7.79	0.81	2.58	0.23	5.28
INGR 28	55.99	0.71	15.73	6.38	0.08	3.10	9.25	0.53	2.32	0.22	7.54
TCC 2136	66.73	0.99	18.45	5.88	0.02	2.24	0.80	0.28	2.54	0.12	1.95

Table 4 Chemical analyses (SEM) of the red coatings and ceramic bodies (oxide wt%)

	Na_2O	MgO	Al_2O_3	SiO_2	K_2O	CaO	TiO_2	FeO
INGR 4 coating	0.9±0.3	3.0±0.4	15.7±0.6	63.4±2.3	2.1±0.5	7.3±0.6	0.9±0.1	6.8±1.1
INGR 4 body	1.2±0.3	2.9±0.4	17.0±1.8	58.9±1.8	2.7±0.6	9.6±0.9	0.9±0.1	6.7±1.0
INGR 14 coating	0.6±0.1	3.0±0.4	22.5±1.7	55.2±2.4	3.2±0.8	5.0±1.2	1.6±0.2	8.8±1.2
INGR 14 body	0.6±0.2	2.8±0.3	21.9±2.0	57.2±1.7	3.8±0.7	5.3±1.3	1.3±0.2	7.1±0.7
INGR 28 coating	0.6±0.1	2.3±0.3	15.8±1.4	65.0±1.3	2.8±0.2	6.9±0.7	0.6±0.3	5.9±1.2
INGR 28 body	0.8±0.1	2.6±0.2	16.3±1.2	58.6±2.7	3.1±0.3	11.3±2.1	0.9±0.2	6.4±1.4
TCC 2136 coating	bdl	1.9±0.4	23.1±2.0	57.9±3.5	2.2±0.3	1.4±0.7	1.3±0.2	12.3±1.5
TCC 2136 body	0.4±0.1	1.9±0.2	21.2±2.3	66.5±3.7	3.1±1.0	0.6±0.2	1.1±0.2	5.4±0.2
TCC 2157 coating	0.7±0.0	1.7±0.0	26.3±0.7	56.7±0.2	2.1±0.4	1.0±0.2	1.2±0.1	10.7±1.5
TCC 2157 body	0.64±0.3	1.7±0.2	26.3±1.9	61.1±2.8	2.9±0.1	0.7±0.0	1.3±0.1	5.3±0.5

spectrum allowed us to determine the mineral phase present in the pottery specimens. The absorption peaks of quartz were detected in all the samples: the main SiO stretching band at 1,080 cm^{-1}, the shoulder at 1,165 and 512 cm^{-1} and the distinctive doublet at 797 and 777 cm^{-1}. Other minerals were identified in these samples, in particular, albite (1,096, 989, 722, and 425 cm^{-1}) and microcline (1,142, 1,134, 1,053, 729, 646, 584, and 464 cm^{-1}) from the feldspar group, muscovite from the phyllosilicate groups (1,062, 1,022, 990, 1,062, 1,022, 990, 935, 754, 553, 480, and 412 cm^{-1}) and hematite (537 and 475 cm^{-1}) were inferred from the second derivative profiles.

In Fig. 5a, b, the absorption and second derivative profiles of IR spectra of the coating of the same samples are reported so as to highlight the differences in mineralogical composition between the coating and the ceramic body. The coating contains the same constituents as the ceramic body, with a small difference in the intensity of the hematite absorption peak. Minerals of an archaeological artefact can be classified as primary minerals (present in the raw materials and not transformed over a wide temperature range) or firing minerals that were formed during firing (De Benedetto et al. 2002). No firing minerals were observed in the second derivative profiles of the IR spectra of the ceramics investigated. The absence of any firing mineral in the ceramic body clearly indicates that these samples were fired at low temperatures.

Micro-Raman analyses were performed on a limited number of samples, but the results encourage further research into the technical features of the different kinds

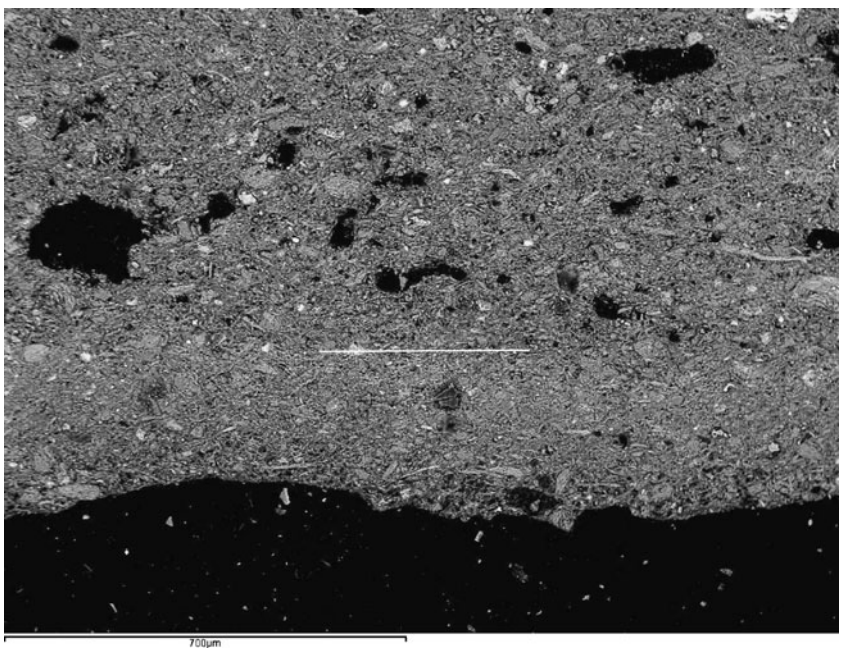

Fig. 3 SEM back scattered electrons image of sample INGR 28 (the *white line* identifies the transition between ceramic body and coating)

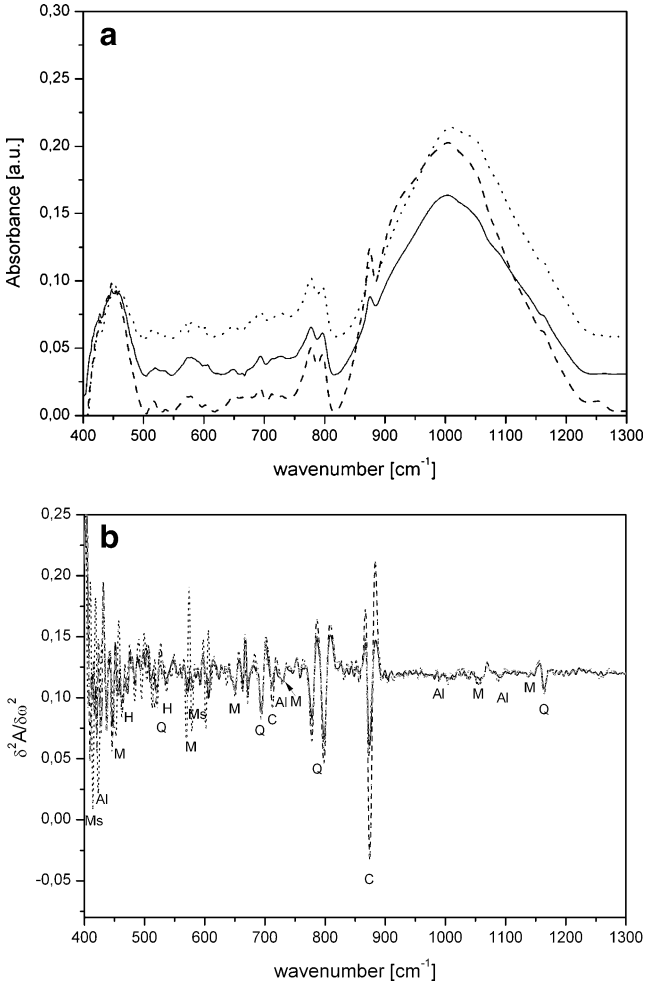

Fig. 4 Infrared spectra of the ceramic body of INGR 24 (*solid line*), INGR 25 (*dashed line*), INGR 27 (*dotted line*) in the region 1,300 and 400 cm^{-1}. **a** Absorption spectrum; **b** second derivative profile. *Al* albite, *C* calcite, *H* hematite, *M* microcline, *Q* quartz, *Ms* muscovite

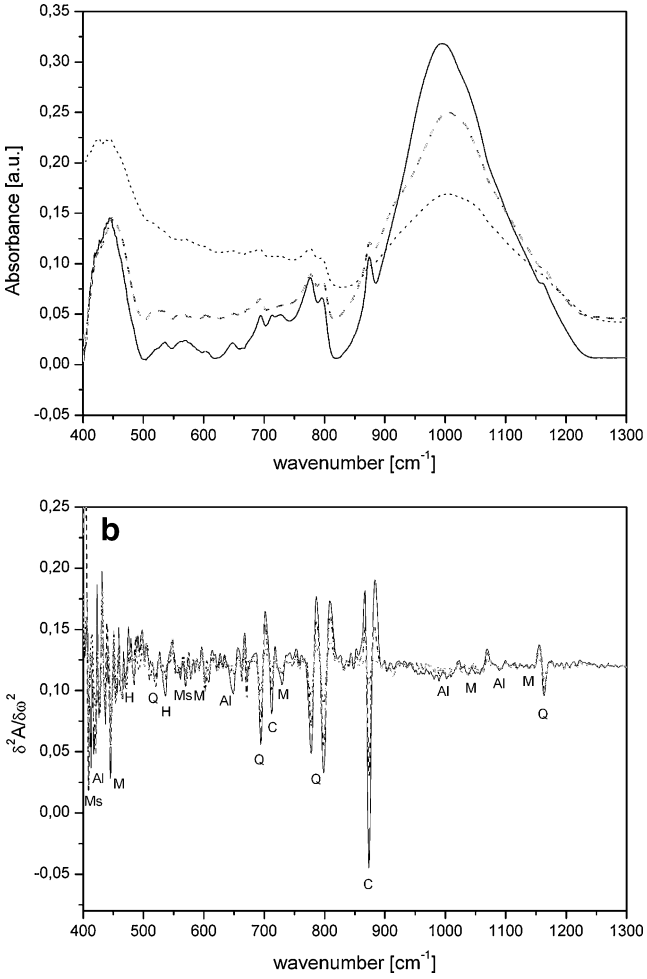

Fig. 5 Infrared spectra of the coating of INGR 24 (*solid line*), INGR 25 (*dashed line*), INGR 27 (*dotted line*) in the region between 1,300 and 400 cm^{-1}. **a** Absorption spectrum; **b** second derivative profiles. *Al* albite, *C* calcite, *H* hematite, *M* microcline, *Q* quartz, *Ms* muscovite

of artefacts. Two specimens of red slip ceramics (INGR5 and INGR27), together with two "similar to African" ceramic findings samples (TCC 2136 and TCC 2157) were examined in order to evaluate the potential of micro-Raman as a complementary technique for studying the different composition of the red coatings.

The usefulness of a micro-Raman investigation of these pottery wares lies in the capacity of this technique to identify and distinguish different iron oxides, even if they are present in small quantities. A valid study of the manufacturing technique is feasible if the behaviour of iron oxide polymorphs is carefully considered. Hematite is the most thermodynamically stable phase under certain firing conditions: at atmospheric pressure, and with temperatures around 380°C γ-Fe_2O_3 particles aggregate, and are transformed into α-Fe_2O_3. In general, no intermediate phases are observed during the thermal treatment of powders, but if micro- and nanoparticles of iron oxides are dispersed in silica matrices, as in the present case, two processes can take place: the stabilization of nanometric γ-Fe_2O_3 particles (Sartoratto et al. 2007, Pérez-Robles et al. 1999), and the formation of ε-Fe_2O_3 as an intermediate phase (Tronc et al. 1998). Previous work (Sartoratto et al. 2007) demonstrated that a silica matrix behaves like an anti-sintering agent: where the temperature of the maghemite particles does not exceed 900–1,000°C the matrix settles them thereby avoiding their thermal transformation into hematite. Above this temperature, mixtures of ε-Fe_2O_3 and α-Fe_2O_3 phases may form.

Figure 6 shows the spectra acquired on various points on the INGR 5 coating. The spectra appear similar, exhibiting the characteristic peaks of hematite (H) at 226, 242, 293, 409, 496, and 611 cm^{-1} (Zoppi et al. 2008). A divergence of the spectra from the hematite spectra provides information on the firing temperature, and also on the substitution of the iron in the hematite structure by different cations.

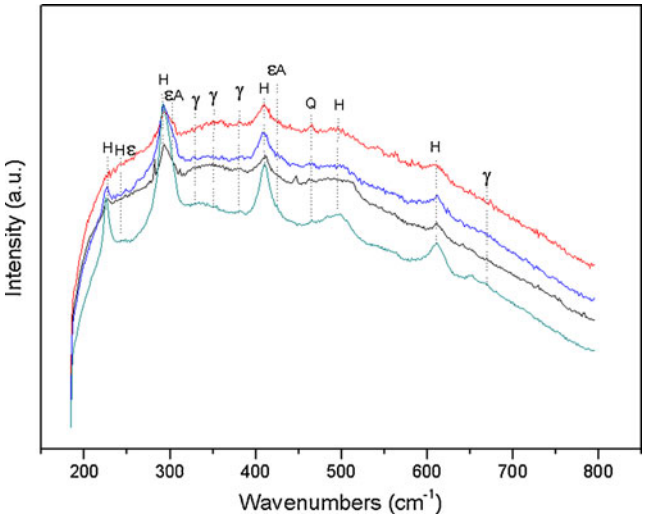

Fig. 6 Raman spectra of four different points on the coating of sample INGR 5: *H* hematite, *ε* ε-Fe_2O_3, *γ* γ-Fe_2O_3, *A* Al-for-Fe-substituted hematite, *Q* quartz

The 328, 354, 380, 496, and 667 cm^{-1} Fe–O stretching modes represent the main evidence of the presence of maghemite (denoted as γ in the spectra) (Chourpa et al. 2005, Colomban et al. 2008). Maghemite (γ-Fe_2O_3) has an inverse spinel structure and can be seen as an iron-deficient form of magnetite. The corresponding Raman bands are not well defined and their widths and position seem to depend on the sample preparation, because they are directly related to the degree of crystallinity of the material.

So the set of the three Raman bands, peaking at 243, 304, and 427 cm^{-1}, may be attributed to the Fe–O stretching modes of the ε-Fe_2O_3 (denoted as ε in the spectra) phase (Sartoratto et al. 2007), which is another polymorph of the iron (III) oxide system. However, the presence of mixed Al-hematite, with an aluminium molar content higher than 4%, should not be excluded, due to the 304 and 427 cm^{-1} Raman bands (Zoppi et al. 2008).

Figure 7 is representative of the spectra registered on the red coating of the INGR 27 sample, indicating the presence of hematite, along with maghemite. In addition to the hematite peaks, the Raman spectra show a broad band at 748 cm^{-1}, attributable to illitic clay (denoted as I in the spectra).

Some spectra from the coating of samples of the "similar to African" type are displayed in Fig. 8. They indicate the presence of hematite only: it is possible that Al cations substitute some Fe cations (Zoppi et al. 2008).

The majority of the spectra from the analysed samples exhibit the features of α-quartz (denoted as Q in the spectra) close to 464 cm^{-1}.

Table 4 reports the FeO and SiO_2 contents of the INGR and TCC samples: the average Fe/Si ratio in the coating is 0.12 in the INGR samples and 0.2 in the TCC samples. This indicates a high silica content for both sets of specimens which suggests that firing temperatures did not reach 1,000 °C. The presence of the maghemite phase, which would have disappeared at higher firing temperatures, supports this.

Another aspect to be taken into consideration is the Na content, which in the INGR samples is quite low. This results in the stabilization of the maghemite phase upon heating to 900°C (Sartoratto et al. 2007). As the spectra of the INGR samples show both maghemite and hematite peaks, it is possible to affirm that the maghemite was not completely transformed into hematite which suggests that the firing temperatures were probably lower than 900°C (Sartoratto et al. 2007). This assumption is confirmed by the presence of illite (Leon et al. 2010). If heated to 1,200°C

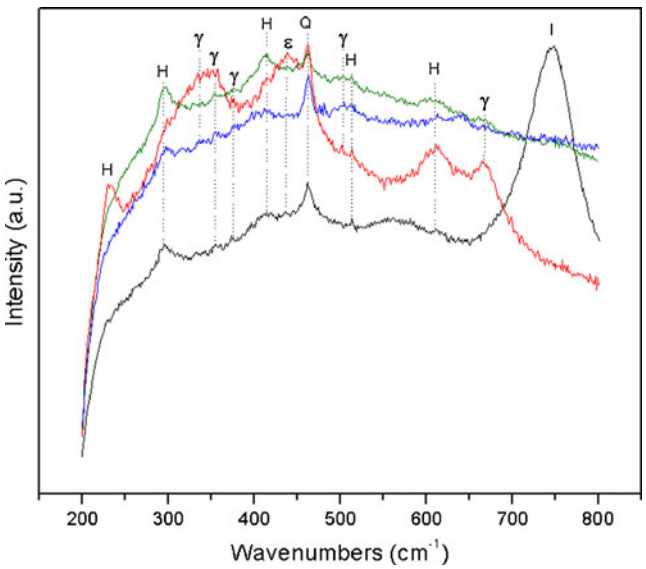

Fig. 7 Raman spectra of four different points on the coating of sample INGR 27: *H* hematite, *ε* ε-Fe_2O_3, *γ* γ-Fe_2O_3, *Q* quartz, *I* illite

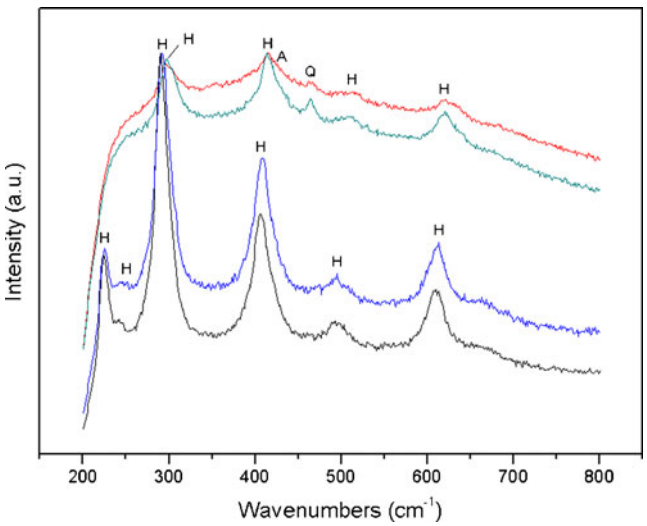

Fig. 8 Raman spectra of four different points on the coating of sample TCC 2136: *H* hematite, *ε* ε-Fe_2O_3, *γ* γ-Fe_2O_3, *A* Al-for-Fe-substituted hematite, *Q* quartz

Table 5 Petrographical description of red slip ceramics (Qz=quartz, Kf=Kfeldspar, Pl=plagioclase, PX=pyroxene)

Sample	Matrix	Skeleton								Porosity
Name	Appearance	Amount	Grain size	Sorting	Qz	Kf	Pl	Px	Other	
INGR 2	Anisotropic	Scarce	<50 μm	Well sorted	X	–	X	tr	–	Scarce oriented
INGR 4	Anisotropic	Very scarce	<50 μm	Well sorted	X	–	X	tr	Micas	Scarce oriented
INGR 5	Anisotropic	Scarce	<50 μm	Well sorted	X	–	X	tr	–	Scarce oriented
INGR 9	Anisotropic	Scarce	50–100 μm	Well sorted	X	X	X	–	–	Medium oriented
INGR 10	Anisotropic	Scarce	50–100 μm	Well sorted	X	X	X	–	–	Medium oriented
INGR 14	Anisotropic	Scarce	<50 μm	Well sorted	X	–	X	–	Chamotte	Medium
									Secondary calcite	Not oriented
INGR 24	Anisotropic	Scarce	<50 μm	Well sorted	X	–	X	–	–	Medium oriented
INGR 25	Anisotropic	Scarce	<50 μm	Well sorted	X	X	X	–	Fossils	Scarce
										Not oriented
INGR 26	Anisotropic	Scarce	50–100 μm	Well sorted	X	X	X	–	Secondary calcite	Medium oriented
INGR 27	Anisotropic	Scarce	<50 μm	Well sorted	X	X	X	–	Secondary calcite	Scarce oriented
INGR 28	Anisotropic	Scarce	<50 μm	Well sorted	X	–	X	tr	Secondary calcite	Scarce oriented
TCC 2136	Anisotropic	Medium	Max 250 μm	Medium sorted	X	tr		–	–	Scarce
			Min 20 μm							Not oriented
TCC 2157	Anisotropic	Medium	Max 250 μm	Medium sorted	X	–	–	–	–	Scarce
			Min 20 μm							Not oriented

and 1,400°C, the bands relative to the maghemite phase disappear and there is a blue shift in the hematite peaks. This suggests that the bands at 304 and 430 cm^{-1} are due to the presence of Al (denoted as A in the spectra) as the substituent cation for Fe in the hematite.

It is possible to conclude that the TCC samples were fired at temperatures higher than 900°C: no peaks referring to maghemite phase were evidenced in their Raman spectra and this means the maghemite must have been completely transformed into hematite. The spectra reported in Fig. 8 show the peaks corresponding to hematite, in some cases red-shifted and broadened, with an additional shoulder located near 430 cm^{-1}, which could be due to the effect of Al-for-Fe replacement in the hematite crystals (Zoppi et al. 2008).

The petrographical analyses using thin sections (OM) (Table 5) confirm the micro-chemical and mineralogical data for the red slip ceramics; the material used for the ceramic bodies appears to be depurated, well sorted and with no temper because of the minimal skeleton (maximum grain size 100 μm) (Fig. 9a). The grains are made up of quartz, plagioclase, rare pyroxene, K-feldspar and hematite. A fragment of chamotte is present in the INGR 14 sample. The calcite is clearly due to secondary precipitation phenomena in the INGR 14, INGR 26, INGR 27, and INGR 28 samples. An analysis of the coating shows that it was obtained using finer but unevenly distributed material and that it is less porous than the body.

In the TCC 2136 and TCC 2157 samples, the body is characterized by an average amount of quartz. This quartz is uniformly distributed throughout the body and has a bimodal grain-size distribution (maximum grain size, 250 μm and minimum grain size, 50 μm) (Fig. 9b) and a sub-spherical shape. The coating is very fine grained, sometimes it remains unsolvable under polarised microscope and its thickness is less than 100 μm.

A cross section of the two groups of red slip ceramics is reported in Fig. 10a, b in order to underline their different aspect and the strong adhesion of the coating to the body.

Uncoated ceramics (coarse pottery)

The mineralogical composition of the coarse pottery, obtained using XRD, is reported in Table 6.

The most important tool for analysing the coarse pottery was OM which provided highly relevant information on its mineralogical and textural characteristics.

All the samples present quartz and plagioclases, except the AG 4 sample, which featured the presence of calcite. The AG C6 sample has a mineralogical association with quartz, plagioclases, phyllosilicates, and K-feldspar, while phyllosilicates are absent in the AG 38 sample. Pyroxenes and amphiboles were detected in several samples as were hematite and calcite.

The use of a large quantity of temper consisting of minerals and rock fragments is evident. The degree of abundance and the kind of temper used enable the different samples to be distinguished according to their function, i.e. the AG 4 sample (casserole) contains only calcitic temper,

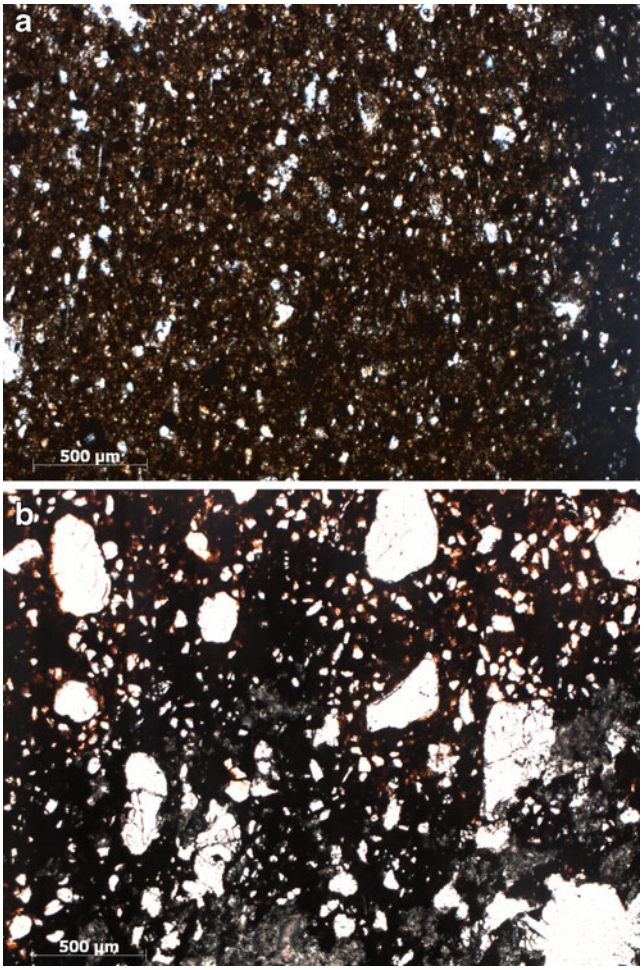

Fig. 9 Photomicrographs of thin section of ceramic body of samples INGR 28 (**a**) and TCC 2136 (**b**) under polarised microscope (*n*//, magnification, 5×)

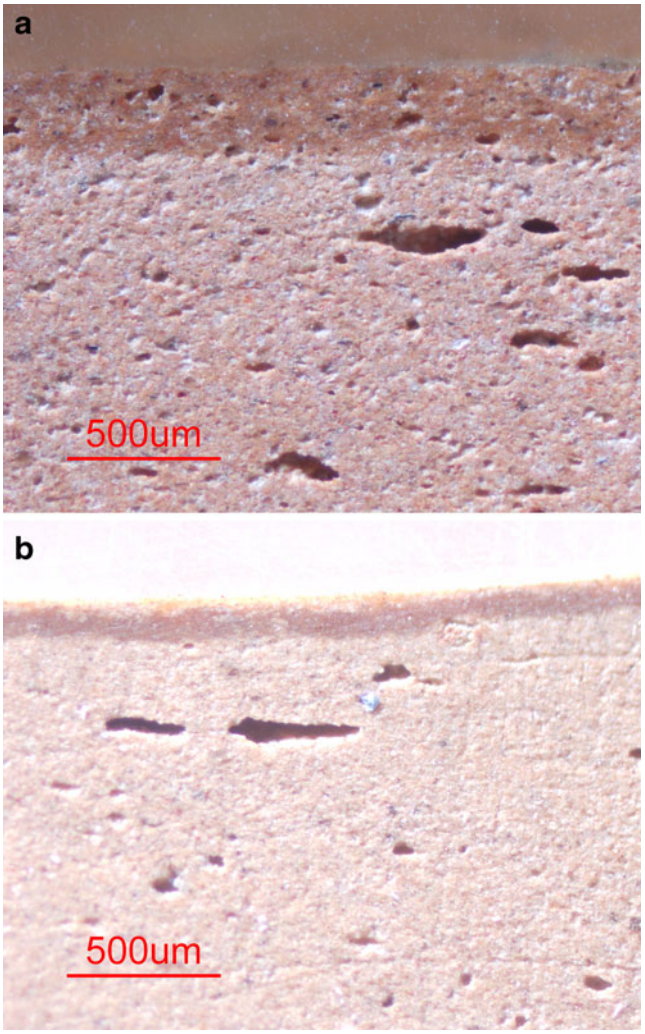

Fig. 10 Cross sections of INGR (**a**) and TCC (**b**) samples

with a typical bimodal distribution, while the AG C6 sample (bowl lid) contains a temper made up of mono and polycrystalline quartz aggregates as well as tiny amounts of plagioclase, k-feldspar and chamotte. The AG 38 sample (cooking pot) shows a well-sorted skeleton consisting of quartz with only two fragments of marble. A large number of samples are characterized by large crystals of plagioclases, clinopyroxenes (augite and diopside), and amphiboles (ferroactinolite and hornblende), and large fragments of marble. Table 7 shows the petrographical description of the samples. Figure 11a–d shows some examples of the varieties of texture and composition in the samples examined.

SEM-EDS analyses proved to be very useful for obtaining information about the composition of the single mineral or rock fragments constituting the temper, for identifying alteration phenomena, for comparing how the composition of the temper varies between the different samples and for highlighting the different kinds of temper in every sample. The temper was characterized by analysing single minerals and the matrix was characterized using areal analyses.

The results of the SEM-EDS analyses showed that the temper used was constituted by pyroxenes and plagioclases obtained most probably crushing magmatic rocks and by calcitic marbles. The analyses of the plagioclases evidenced a prevalently albitic-oligoclasic composition, and pronounced alteration phenomena (i.e. calcite and zoisite), while the pyroxenes contained Ca–Fe–Mg. It is important to stress that the mosaic *tesserae* of the Roman *villa* contain abundant fragments of white and yellow marbles, veined marbles and magmatic rocks (*Lapis Laecedaemonius* or green porphyry and *Lapis Porphyrites* or red porphyry). These results would seem to suggest that material (i.e. marble) from the destroyed *villa* was reutilized to make ceramic temper. To provide further evidence of this hypothesis, a thin section of the AG C9 sample (Fig. 12a), with an evident fragment of marble added as

Table 6 Mineralogical composition of coarse pottery

Sample	Quartz	Plagioclase	K-feldspar	Micas	Pyroxene	Hematite	Calcite	Amphibole
AG2	X	X	–	X	X	X	X	–
AG4	tr	tr	–	tr	–	–	X	–
AG23	X	X	–	X	X	–	X	X
AG28	X	X	–	X	X	X	–	–
AGC4A	X	X	–	–	X	X	X	X
AGC5	X	X	–	X	X	–	X	X
AGC6	X	X	X	X	–	–	–	–
AGC7	X	X	–	X	X	X	X	–
AGC8	X	X	–	X	X	–	tr	X
AGC9	X	X	–	–	X	X	X	X
AGC10	X	X	–	–	X	–	tr	tr
AGC13	X	X	–	–	X	–	–	X
AG32	X	X	–	X	X	X	X	X
AG33	X	X	–	X	X	X	X	tr
AG34	X	X	–	X	X	X	X	tr
AG35	X	X	–	X	X	X	X	X
AG36	X	X	–	X	X	X	tr	X
AG37	X	X	–	X	X	X	tr	X
AG38	X	X	–	X	–	–	–	–
AG39	X	X	–	tr	X	X	–	X
AG40	X	X	–	tr	X	X	–	tr

temper is compared with three thin sections (Fig. 12b–d) of white marbles with different grain size pertinent to the Roman *villa*.

SEM-EDS analyses were also used to ascertain the composition of the ceramic bodies of the coarse pottery. In Table 8, the main composition of the ceramic bodies is reported as mean measurements from 12 different areas of each sample (single area is 20×30 μm), carefully avoiding the temper.

The ceramic body samples all have a similar chemical composition: only the amount of K_2O varies, probably because of a variation in the clayey raw material.

Comparing the red slip ceramics and the coarse pottery

The results of the chemical analysis of all the ceramic bodies (the AG, INGR, and TCC samples) carried out using SEM-EDS, are synthesized in binary (Fig. 13a–d) and in ternary (Fig. 14) plots. The AG areas investigated were carefully selected to ensure there was no temper; homogeneous internal areas were used for the INGR and TCC specimens.

A comparison of all the samples demonstrates that the ceramic body composition is quite similar for the INGR and AG samples while the TCC samples are clearly different.

From binary diagrams (SiO_2/Al_2O_3, SiO_2/MgO, SiO_2/K_2O, and SiO_2/Na_2O) (Fig. 13a–d), some of these differences can be clearly observed. The Al_2O_3–SiO_2 diagram shows that the TCC samples have higher values of Al_2O_3 than the AG and INGR samples; in the MgO–SiO_2 diagram the MgO reading for the TCC samples is below 2% whilst in the other samples it is variable, ranging from above 2% up to 7–8%. The K_2O–SiO_2 diagram shows that the values of K_2O are very variable and that the variation does not depend on the group the specimen comes from; in the Na_2O–SiO_2 diagram the Na_2O values are lower in TCC samples (less than 1%) and highest in the AG samples (up to 5%). In the K_2O–SiO_2–Al_2O_3 ternary diagram (Fig. 14), the TCC samples can be distinguished from the AG and INGR samples; the single clustering of the TCC samples is quite evident.

From this description, it is possible to highlight that three groups of ceramics can be distinguishable: TCC, INGR and AG samples. The main chemical differences in the composition of ceramic body allow to distinguish the TCC group with a lower Na_2O, and MgO content and a higher Al_2O_3 content. Also, the AG samples have higher levels of Na_2O and MgO and lower levels of K_2O than the INGR samples while the Al_2O_3 and SiO_2 content of these two sample groups are quite similar.

Table 7 Petrographical description of thin sections of coarse pottery (Qz=quartz, Kf=Kfeldspar, Pl=plagioclase, Px=pyroxene)

Sample	Matrix	Skeleton								Porosity
Name	Appearance	Amount	Grain size	Sorting	Qz	Kf	Pl	Px	Other	
AG2	Anisotropic	Abundant	Max 1 mm	Not well sorted	X		X	X	Micas	Scarce
			Min 50 μm						Marbles	Irregular shape
									ARF	
AG4	Anisotropic	Abundant	Max 1.5 mm	Bimodal	tr	–	–	–	Calcitic fragments	Abundant
			Min 100 μm							Oriented cracks
AG 23	Anisotropic	Abundant	Max 1.5 mm	Not well sorted	X	–	X	X	Marbles	Scarce
			Min 50 μm						Amphiboles	Irregular shape
AG 28	Anisotropic	Abundant	Max 2 mm	Not well sorted	X	–	X	X	Chamotte	Scarce
			Min 50 μm						ARF	Irregular shape
AGC4A	Anisotropic	Abundant	Max 1.2 mm	Not well sorted	X	–	X	X	Marbles	Medium
			Min 50 μm						Amphiboles	Oriented cracks
AGC5	Anisotropic	Abundant	Max 800 μm	Bimodal	X	–	X	X	Marbles	Abundant
			Min 50 μm						Amphiboles	Oriented cracks
AGC6	Anisotropic	Scarce	Max 1 mm	Well sorted	X	X	X	–	Chamotte	Abundant
			Min 50 μm							Irregular shape
AGC7	Anisotropic	Abundant	Max 1.5 mm	Bimodal	X	–	X	X	Marbles	Abundant
			Min 200 μm							Oriented cracks
AGC8	Anisotropic	Abundant	Max 1.5 mm	Bimodal	X	–	X	X	Marbles	Abundant
			Min 200 μm						Amphiboles	Irregular shape
AGC9	Anisotropic	Abundant	Max 1.5 mm	Bimodal	X	–	X	X	Marbles	Medium
			Min 200 μm						Amphiboles	microcracks
AGC10	Anisotropic	Abundant	Max 2 mm	Not well sorted	X	–	X	–	Marbles	Abundant
			Min 200 μm						Amphiboles	Irregular shape
AGC11	Anisotropic	Abundant	Max 400 μm	Not well sorted	X	–	X	–	Marbles	Abundant
			Min 100 μm						Chamotte	Irregular shape
AGC13	Anisotropic	Medium	Max 1 mm	Bimodal	X	–	X	X	Amphiboles	Scarce
			Min 50 μm							Irregular shape
AG 34	Anisotropic	Abundant	Max 1 mm	Medium sorted	X	–	X	X	Marbles	Scarce
			Min 50 μm						Micas	Irregular shape
AG 35	Anisotropic	Abundant	Max 1.2 mm	Medium sorted	X	–	X	X	Marbles	Medium
			Min 50 μm						Micas	Not oriented cracks
AG 36	Anisotropic	Abundant	Max 1.2 mm	Not well sorted	X	–	X	X	Amphiboles	Scarce
			Min 50 μm						ARF	Irregular shape
AG 37	Anisotropic	Medium	Max 1 mm	Not well sorted	X	X	–	X	Marbles	Medium
			Min 50 μm							Not oriented cracks
AG 38	Anisotropic	Medium	Max 500 μm	Well sorted	X	–	–	–	2 fragments of marble	Abundant
			Min 50 μm							Oriented cracks
AG 39	Anisotropic	Medium	Max 1.4 mm	Medium sorted	X	X	–	X	Amphiboles	Medium
			Min 50 μm						ARF	Irregular shape
AG 40	Anisotropic	Abundant	Max 1.2 mm	Not well sorted	X	–	X	X	Amphiboles	Scarce
			Min 50 μm						Micas	Irregular shape

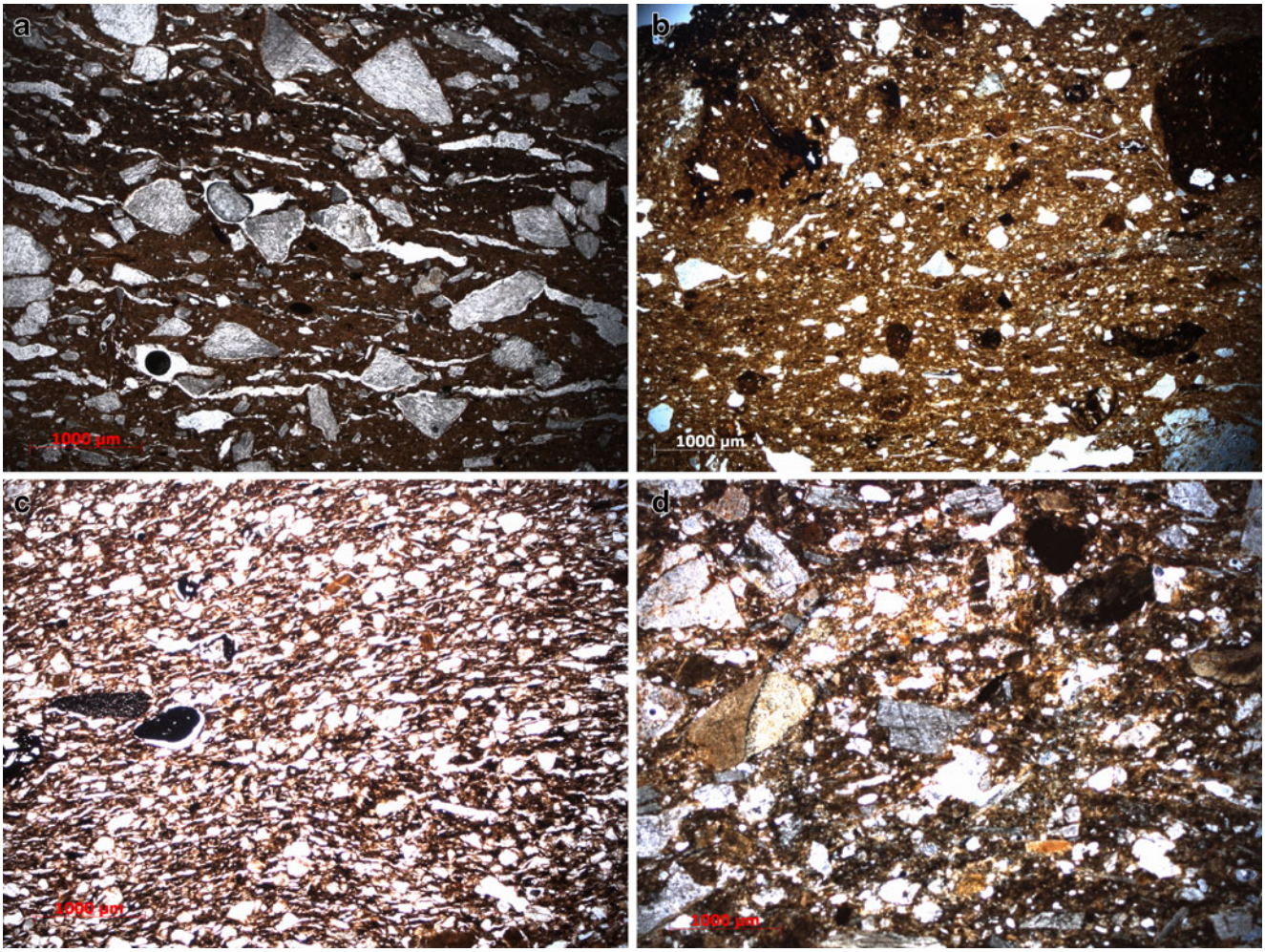

Fig. 11 Photomicrographs of thin sections of the sample AG 4 with evident calcitic added temper with a bimodal grain size distribution and numerous microcracks (**a**); thin section of the sample AG C6 with scarce quartz-feldspatic subangular skeleton and chamotte (**b**); thin section of the sample AG 38 with quite abundant quartz skeleton and numerous pores (**c**); thin section of the sample AG 23 with abundant added temper constituted by quartz, plagioclases, pyroxenes, amphiboles, and rock fragments (**d**), polarised microscope (*n*//, magnification 2.5×)

Conclusions

A residential site, attributable to the high Roman aristocracy, was occupied by a people of Germanic culture (probably Ostrogoths or Lombards) from the sixth AD. The occupiers used the *villa* as a quarry for materials required for their productive activities (ceramics, metals, and glass). The analyses carried out aimed to define the typology, the technological level and the provenance of the raw material used so as to better understand the productive work that characterized the final stage of the *villa*. This study also provides a comparison with other similar local findings and may assist in assessing possible trade products.

The discovery of numerous, highly fragmented ceramic findings directed research firstly towards petrographic, mineralogical analysis with the objective of identifying specific groups, especially for the red slip ceramics; this research was followed by more precisely targeted micro-chemical investigation.

The use of different analytical techniques made it possible to characterize the materials at different scales. The use of bulk chemical or mineralogical techniques alone does not adequately characterize the red slip ceramics because the data obtained on the powders show the mean composition of the samples, with no differentiation between body and coating. Micro-chemical analyses, such as ATR-FTIR, SEM-EDS, and micro-Raman performed on small fragments of the samples made it possible to differentiate the composition and texture of the body and the coating. The red slip ceramics are clearly subdivided into two groups: INGR and TCC. The TCC 2136 and TCC 2157 samples that were fired at high temperature, were probably imported; in fact the temper, observed using OM and SEM-EDS, is made up of well-sorted, rounded quartz fragments

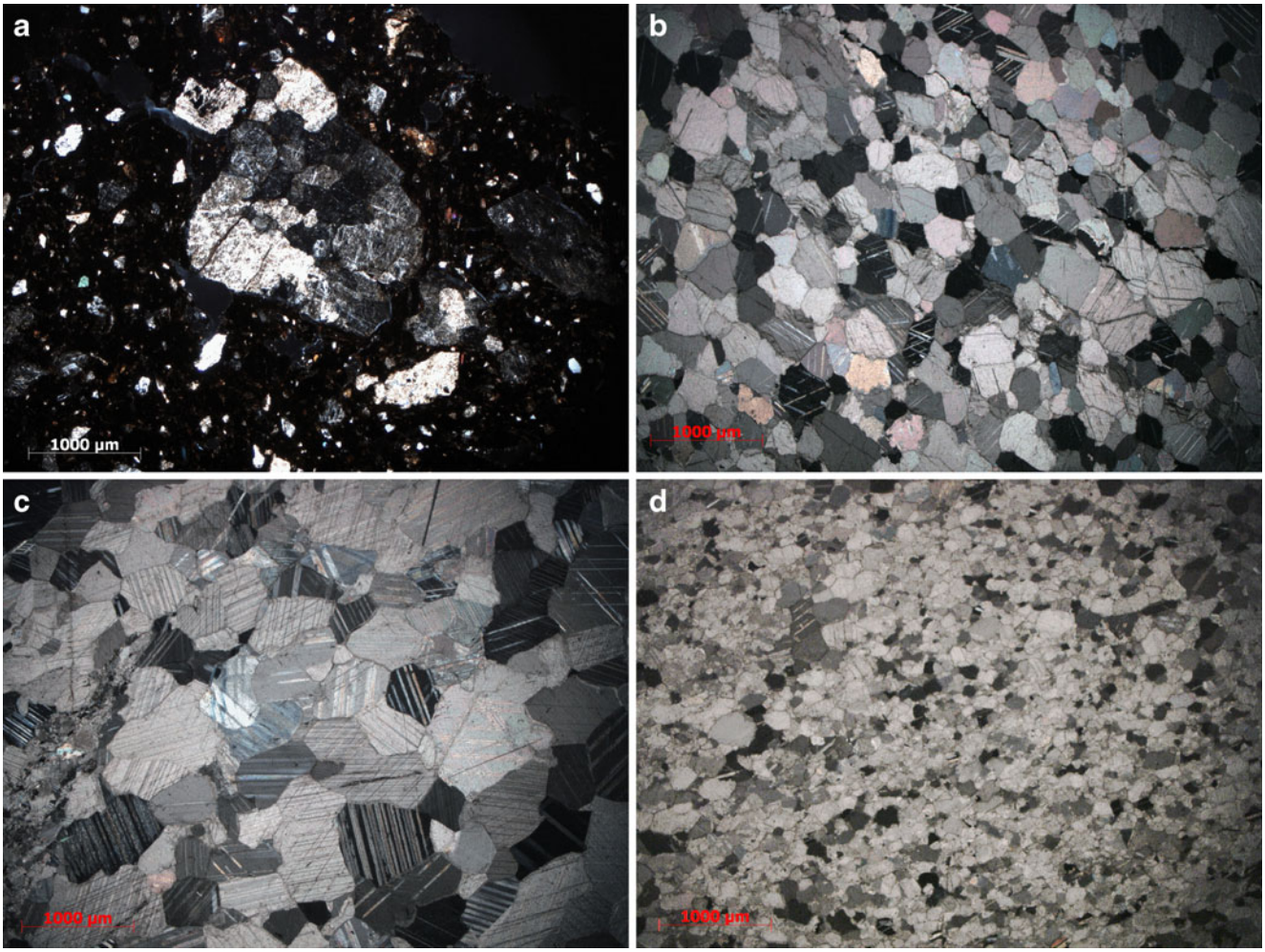

Fig. 12 Photomicrographs of thin section of a calcitic fragment of marble used as temper in the sample AG C9 (**a**); thin sections of three calcitic white marbles pertinent to the Roman *villa*, with different grain size that could be used in the ceramic as temper after crushing (**b**–**d**) (*n*^, magnification 2.5×)

(frequently found in African territory), and the coating is characterized by a significant Fe enrichment. There is no clear chemical or mineralogical difference between coating and body in the INGR samples especially as regards the amount of Fe present; the most relevant difference between these samples is their grain size: smaller in the coating than it is in the body. This coating seems to have been obtained from well-sorted clayey raw material. These INGR ceramic samples were produced using low firing temperatures.

The coarse pottery was subjected to XRD, OM, and SEM-EDS analyses: these analyses were performed on both the body and the added temper. Material coming from the mosaic *tesserae* of the Roman *villa* may have been reutilized as temper for these ceramics. This would suggest that the clayey raw materials were probably extracted from local outcrops: if the temper were obtained from materials coming from the *villa*, it would be logical to hypothesize the use of local clay as the raw material. A comparison of the data relative to the AG and INGR bodies supports this hypothesis: the SiO_2 and Al_2O_3 values are similar whilst the K_2O, Na_2O, and MgO values are heterogeneous. Such results are not inconsistent with

Table 8 SEM-EDS chemical analyses (oxide wt.%) of bodies of coarse pottery samples (mean measurements from 12 different areas)

Sample	Na_2O	MgO	Al_2O_3	SiO_2	K_2O	CaO	TiO_2	FeO
AG28 body	2.7±0.8	4.9±1.2	19.3±0.6	60.2±2.0	0.7±0.1	4.4±0.8	0.7±0.2	7.3±0.9
AG 2 body	2.8±1.0	5.3±3.6	18.1±1.0	60.61±5.0	1.6±0.3	3.8±0.8	0.7±0.1	7.1±1.9

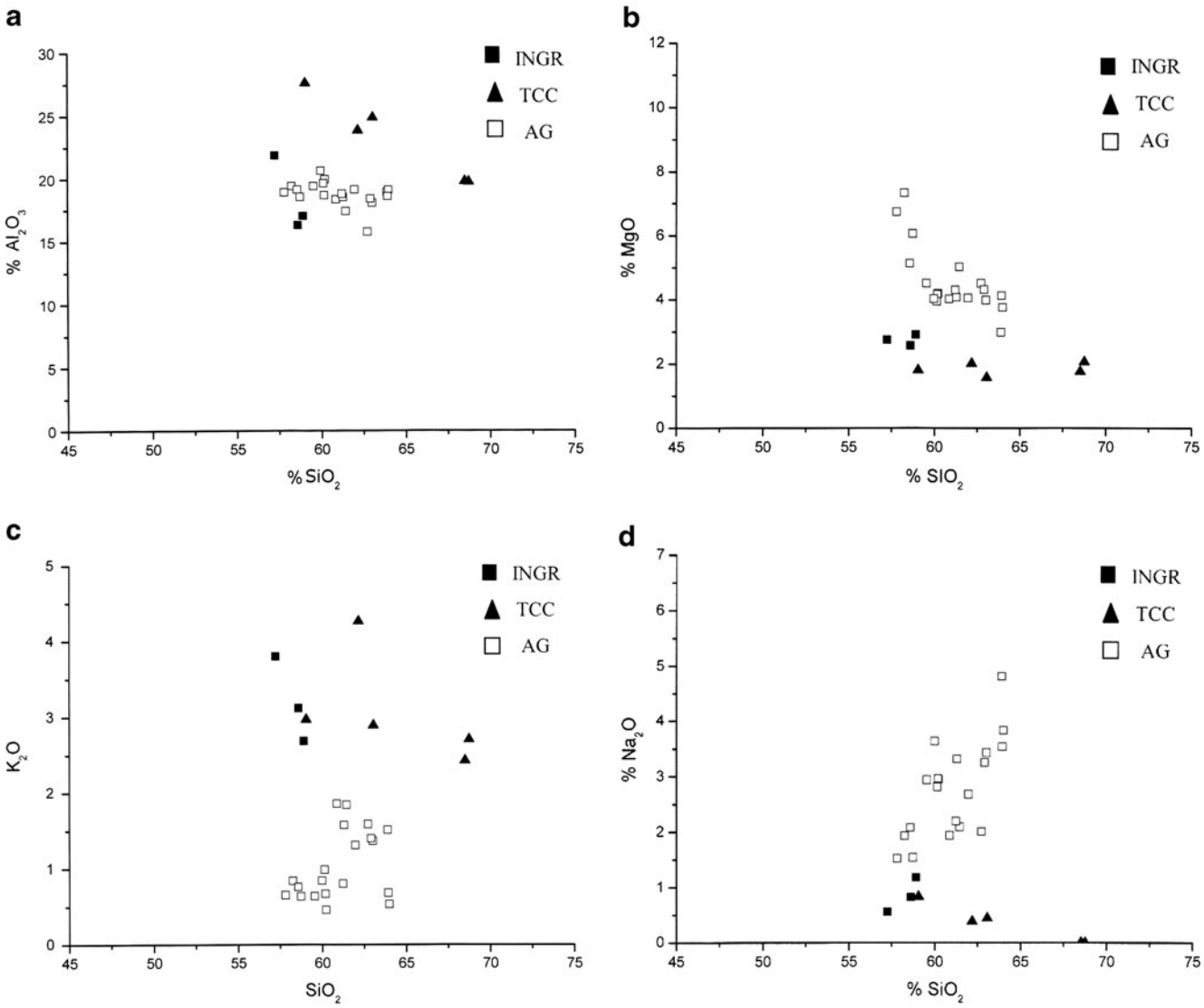

Fig. 13 **a**–**d** Binary diagrams on ceramic bodies of AG, INGR, and TCC samples (SiO_2–Al_2O_3; SiO_2–MgO; SiO_2–K_2O; and SiO_2–Na_2O)

mineralogically varied compositions within a given clayey outcrop utilized for ceramic production. Analyses of different local outcrops of clayey material in the area are planned.

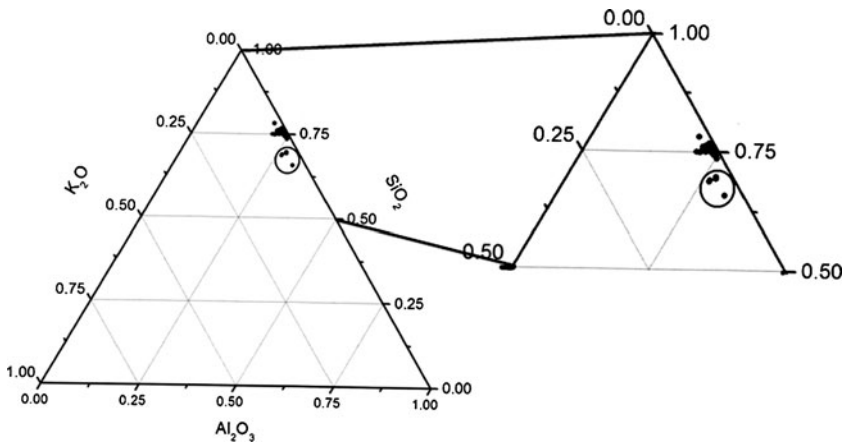

Fig. 14 Ternary diagram (SiO_2–Al_2O_3–K_2O); *in the circle*, the samples TCC

Acknowledgements The authors would like to thank Daniele De Luca for the preparation of samples and Giacomo Baldini, Enrica Boldrini, Charles Bossu, Antonia Fumo, and Paola De Idonè for archaeological suggestions.

References

Cavalieri M (2009a) "Il pavimento in cementizio della villa tardoantica di Aiano-Torraccia di Chiusi (Siena). Primi dati su decorazione musiva, tecnica esecutiva e orizzonte cronologico". In: Atti del XV Colloquio dell'AISCOM, Aquileia, 7–4 February 2009, pp 515–526

Cavalieri M (2009b) "Vivere in Val d'Elsa tra tarda Antichità e alto Medioevo. La villa romana di Aiano-Torraccia di Chiusi (Siena, Italia)". The Journal of Fasti Online AIAC. Available at www.fastionline.org/docs/FOLDER-it-2009-156.pdf

Cavalieri M, Boldrini E (2008) "La villa tardoantica di Aiano-Torraccia di Chiusi (San Gimignano, Siena-Italia) I materiali ceramici: primi dati archeologici ed archeometrici". In: 3rd international conference on late Roman coarse wares, cooking wares and amphorae in the Mediterranean: archaeology and archaeometry. Comparison between Western and Eastern Mediterranean, Parma/Pisa, 26–30 March 2008

Cavalieri M, Giumlia-Mair A (2009) Lombardic Glass working in Tuscany. Mater Manuf Process 24(9):1023–1032

Chourpa I, Douziech-Eyrolles L, Ngaboni-Okassa L, Fouquenet JF, Cohen-Jonathan S, Soucé M, Marchaisb H, Duboisa P (2005) Molecular composition of iron oxide nanoparticles, precursors for magnetic drug targeting, as characterized by confocal Raman microspectroscopy. Analyst 130:1395–1403

Colomban P, Cherifi S, Despert G (2008) Raman identification of corrosion products on automotive galvanized steel sheets. J Raman Spectrosc 39(7):881–886

Cuomo di Caprio N (2007) Ceramica in archeologia 2. L'Erma di Bretschneider, Rome

De Benedetto GE, Laviano R, Sabbatini L, Zambonin PG (2002) Infrared spectroscopy in the chemical and mineralogical characterization of ancient pottery. J Cult Herit 3:177–186

Fabbri B (1998) "The problem of defining the firing temperature of ceramic artefacts". In: Proceedings of XIII Union Internationale des Sciences Préhistoriques et Protohistoriques, Forlì (Italy), September 1996, 1:207–214

Farmer VC (ed) (1974) Infrared spectra of minerals. Mineralogical Society, London

Franzini M, Leoni L, Saitta M (1975) Revisione di una metodologia analitica per fluorescenza-X, basata sulla correzione completa degli effetti di matrice. Rendiconti Società Italiana di Mineralogia e Petrologia 31:365–378

Fumo A (2010) "Le ceramiche rivestite di rosso della villa di Aiano-Torraccia di Chiusi (San Gimignano, Siena): uno studio archeologico e archeometrico". The Journal of Fasti Online AIAC. Available at http://www.fastionline.org/docs/FOLDER-it-2010-178.pdf

Hayes JW (1972) Late Roman Pottery. British School at Rome, London

Leon Y, Lofrumento C, Zoppi A, Carles R, Castellucci EM, Sciau P (2010) Micro-Raman investigation of terra sigillata slips: a comparative study of central Italian and southern Gaul productions. J Raman Spectros 141(1):1550–1555. doi:10.1002/jrs.2678, Published online in Wiley Interscience: (www.interscience.wiley.com)

Maggetti M (1982) Phase analysis and its significance for technology and origin. In: Franklin AD, Olin JS (eds) Archaeological Ceramics. Smithsonian Institution Press, Washington, pp 121–133

Maggetti M (1994) "Mineralogical and petrographical methods for the study of ancient pottery" In: Burragato F, Grubessi O, Lazzarini L (eds) 1st European workshop on archaeological ceramics, Rome, 10–12 October 1991, pp. 23–35

Pecchioni E, Cantisani E, Pallecchi P, Fratini F, Buccianti A, Pandeli E, Rescic S, Conticelli S (2007) Characterization of the amphorae, stone ballast and stowage materials of the ships from the archaeological site of Pisa-San Rossore, Italy: inferences on their provenance and possible trading routes. Archaeometry 49(1):1–22

Pérez-Robles F, García-Rodríguez FJ, Jiménez-Sandoval S, González-Hernández J (1999) Raman study of copper and iron oxide particles embebbed in an SiO_2 matrix. J Raman Spectrosc 30:1099–1104

Sartoratto PPC, Caiado KL, Pedroza RC, da Silva SW, Morais PC (2007) The thermal stability of maghemite-silica nanocomposites: an investigation using X-ray diffraction and Raman spectroscopy. J Alloys Compd 434:650–654

Tite MS (1999) Pottery production, distribution and consumption. The contribution of physical sciences. J Archaeol Method Theory 6:181–233

Tronc E, Chanéac C, Jolivet JP (1998) Structural and magnetic characterization of ε-Fe_2O_3. J Solid State Chem 139:93–104

Turbanti Memmi I (2004) Pottery production and distribution: the contribution of mineralogical and petrographical methodologies in Italy. State of the art and future developments. Periodico di Mineralogia 73:239–257

Zoppi A, Lofrumento C, Castellucci EM, Sciau P (2008) Al-for-Fe substitution in hematite: the effect of low Al concentrations in the Raman spectrum of Fe_2O_3. J Raman Spectrosc 39:40–46